IRIS AperTO

UNIVERSITÀ DEGLI STUDI DI TORINO

AperTO - Archivio Istituzionale Open Access dell'Università di Torino

Hydrogenation of ethylene over palladium: Evolution of the catalyst structure by: Operando synchrotron-based techniques

This is a pre print version of the following article:

Original Citation:

Availability:

This version is available http://hdl.handle.net/2318/1838421 since 2022-02-03T22:51:13Z

Published version:

DOI:10.1039/c9fd00139e

Terms of use:

Open Access

Anyone can freely access the full text of works made available as "Open Access". Works made available under a Creative Commons license can be used according to the terms and conditions of said license. Use of all other works requires consent of the right holder (author or publisher) if not exempted from copyright protection by the applicable law.

(Article begins on next page)

14 October 2023

Hydrogenation of ethylene over palladium: Evolution of the catalyst structure by operando synchrotron-based techniques

Aram L. Bugaev,*[a,b] Oleg A. Usoltsev,[a,b] Alexander A. Guda,[a] Kirill A. Lomachenko,[c] Michela Brunelli,[c] Elena Groppo,[d] Alexander V. Soldatov,[a] Riccardo Pellegrini,[e] Jeroen A. van Bokhoven[f,g]

Palladium-based catalysts are exploited in the industrial scale for selective hydrogenation of hydrocarbons. Formation of palladium carbide and hydride phases under reaction conditions changes the catalytic properties of the material, which points to the importance of *operando* characterization for determining a relation between the relative fraction of the two phases and the catalyst performance. We present a combined time-resolved characterization by X-ray absorption spectroscopy (in both XANES and EXAFS regions) and X-ray diffraction of the working Pd-based catalyst during hydrogenation of ethylene in a wide range of partial pressures of ethylene and hydrogen. Synergetic coupling of three techniques allowed us to follow the structural evolution of Pd lattice as well as the transitions between metallic, hydride and carbide phases of palladium. Nanometric dimensions of the particles resulted in the considerable contribution of both surface and bulk carbides in the absorption spectra. Unusual contraction of the cell parameter of Pd lattice in the spent catalyst was observed upon increasing hydrogen partial pressure.

[a.] *The Smart Materials Research Institute, Southern Federal University, Sladkova 178/24, 344090, Rostov-on-Don, Russia Email: abugaev@sfedu.ru*

[b.] *Southern Scientific Centre, Russian Academy of Sciences, Chekhova 41, 344006 Rostov-on-Don, Russia*

[c.] *European Synchrotron Radiation Facility, 71 avenue des Martyrs, CS 40220, 38043 Grenoble Cedex 9, France*

[d.] *Department of Chemistry and NIS Interdepartmental Centre, University of Turin, via P. Giuria 7, 10125 Turin, Italy*

[e.] *Chimet SpA - Catalyst Division, Via di Pescaiola 74, 52041 Viciomaggio Arezzo, Italy*

[f.] *Institute for Chemical and Bioengineering, ETH Zurich, Vladimir-Prelog-Weg 1, 8093 Zurich, Switzerland*

[g.] *Laboratory for Catalysis and Sustainable Chemistry, Paul Scherrer Institute, 5232 Villigen, Switzerland*

† Electronic Supplementary Information (ESI) available [XRPD analysis; XANES spectra].
See DOI: 10.1039/x0xx00000x

1. Introduction

Palladium-based catalysts are extensively used in industrial applications to selectively hydrogenate alkynes in the alkyne/alkene mixtures.[1-3] In particular, ethylene polymerization requires selective semi-hydrogenation of acetylene in the ethylene-rich mixtures avoiding full hydrogenation to ethane.[4] Being a problem of high fundamental and industrial importance, understanding the conditions which govern the activity and selectivity of the catalyst attracted scientific interest in different times. It was observed that exposure of the catalyst to hydrogen/hydrocarbon mixtures may lead to formation of hydride and carbide phases of palladium,[2] which affects its catalytic activity and selectivity. However, the exact role of hydrides and carbides in the activity and selectivity, as well as the molecular-level picture of the catalytic hydrogenation over palladium, are still under debate.

In a number of studies, bulk absorbed hydrogen was claimed to be responsible for non-selective full hydrogenation of alkynes to alkanes.[5-8] According to Teschner and co-authors[7, 8] the hydrogenation of alkynes leads to formation of PdC phase in the subsurface layers, while the same procedure with alkenes do not induce any modifications in the subsurface region. As the result of extensive studies reviewed by Armbrüster et al.,[1] it was concluded that the PdC phase is responsible for selective partial hydrogenation of alkynes to alkenes, while absence of Pd-C on the surface leads to unselective total hydrogenation of alkynes and alkenes to alkanes. However, most of these results were obtained at low (~1 mbar) partial pressures of the reactants, and the interpolation to the atmospheric pressures is not always straightforward.[2, 3]

In the alternative studies of Tew et al.,[9, 10] palladium carbide phase was formed during both selective and non-selective hydrogenation of 1-pentyne. In particular, at 100 °C the selectivity to pentane was 72 %, while the observed structure of the catalyst corresponded to the palladium carbide. Pradier et al observed that the β-PdH phase provided selectivity of ethylene formation over 90%. Borodziński et al.[11] investigated Pd/Al_2O_3 catalyst at pressures about 0.3 bar and concluded that the decomposition of β-PdH improved the selectivity to semi-hydrogenation, but at the same time the rate of ethane formation was increased by one order. In the same work it was also observed that in presence of hydrocarbons β-PdH is formed under much higher partial pressures of hydrogen comparing to Pd-H phase diagram obtained with pure hydrogen,[12] which indicates that an investigation of Pd-H/Pd-C phase diagram under different partial pressures of hydrogen and hydrocarbon molecules is required. In our recent works, formation of palladium carbides was observed in presence of acetylene,[13, 14] ethylene[14, 15] and under reaction conditions,[15, 16] which also highlighted irreversible changes in the catalyst structure in the time scales from minutes to hours.

In the current work, we performed *operando* time-resolved study of supported Pd nanoparticles during ethylene hydrogenation reaction by combined Pd *K*-edge extended X-ray absorption fine structure (EXAFS) spectroscopy, X-ray absorption near edge structure (XANES) spectroscopy, X-ray powder diffraction (XRPD) and mass spectrometry. Finally, an unusual behaviour was observed in the spent catalyst exposed to an excess of hydrogen.

2. Experimental and methods

2.1. Sample characterization

The industrial palladium-based catalyst was provided by Chimet S.p.A.[17-19] The synthesis was performed following the deposition–precipitation method using an activated carbon[20] as a support. According to TEM characterization, the average nanoparticle size in the sample is 2.6 nm.[13]

2.2. Synchrotron measurements

Synchrotron-based measurements were performed at the BM31 beamline[21, 22] of ESRF (Grenoble, France). The catalyst in the form of powder was loaded in a glass capillary with inner diameter of 1.0 mm. Having the total length inside the capillary of ca. 5 mm, the catalyst was fixed from both sides by quartz wool. Remotely controlled gas setup (See Figure S1 of ESI) with three mass flow controllers (MFC), responsible for helium, hydrogen and ethylene fluxes, was connected to the inlet of the capillary. The gas mixture was flowed under atmospheric pressure, the overpressure was being controlled by a pressure gauge connected before the capillary. A total flux of 50 mL/min was conserved during the whole experimental procedure. The outlet of the capillary was connected to a Pfeiffer OmniStar GSD 320 online mass spectrometer (MS). Gas blower positioned above the sample was used to control the temperature. The sample activation was performed at 125 °C in 4:1 He/H_2 mixture for 30 minutes. Then, the sample was cooled down to 80 °C and during the following experimental steps the partial pressures of the three gasses were changed stepwise by means of mass flow controllers (See Figure S2).

At each step, X-ray absorption and X-ray powder diffraction data were quasi-simultaneously collected. X-ray absorption spectra at Pd *K*-edge were obtained in the transmission geometry by ionization chambers in the continuous scanning mode with simultaneous measurement of Pd foil for energy calibration. X-ray diffraction was measured using 0.50522 Å radiation by CMOS-Dexela 2D detector, the geometry used allowed to get diffraction pattered in the 2θ range from 2 to 51 degrees. The beamline allowed fast switching between XAS and XRD regimes, so that the total time needed for single X-ray absorption and diffraction measurement was about 20 minutes.

2.3. Data analysis

Single-shell Fourier analysis of EXAFS was performed using the Demeter 0.9.21 package.[23] A real space data fitting in the R-range from 1.5 to 3.2 Å was performed on the k^2-weighted data in the *k*-range from 5 to 12 $Å^{-1}$. Theoretical amplitudes and phases functions were calculated by FEFF6 code.[24] The fit included four parameters: Pd-Pd interatomic distance ($R_{Pd\text{-}Pd}$), the Debye-Waller factor (σ^2), energy shift (ΔE_0) and coordination number (N). The parameters ΔE_0 and N were considered as common variables for all spectra. The value of the reduction factor $S_0^2 = 0.82$ was obtained by fitting the spectrum of the palladium foil.

PCA analysis of the XANES spectra was performed in PyFitit code[25] to determine the number of independent components. Then, the SIMPLISMA approach[26] was applied with subsequent linear combination fit of all experimental spectra.

The initial 2-dimentional X-ray diffraction images were processed in PyFAI code[27, 28] which allows fast averaging, background subtraction and integrating to obtain $I(2\theta)$ patterns. Rietveld refinement was performed in Jana2006 program.[29] Profile parameters were obtained by fitting the patterns of pure and the most hydrated samples at each temperature. The fitted variables were the ratio between α- and β-phases and cell parameters corresponding to each of these phases.

For the mass spectroscopy data analysis, we used the ratio of m/Z = 30 and 28 to quantify the conversion of ethylene. This approach allowed us to overcome the problem of similar mass-spectra of ethylene and ethane molecules, while the ratio of the two m/Z signals varies from 0 for pure ethylene to ca. 0.25 for pure ethane.[15]

3. Results

3.1. Evolution of the atomic and electronic structure of the catalyst during ethylene hydrogenation followed by combined XRPD/EXAFS/XANES

The experimental conditions are summarized in Figure 1a. The whole experiment was performed at 80 °C. Initially, the activated catalyst was exposed to various H_2/He flows and concentrations (region I in Figure 1) to (i) reproduce the phase transition between metallic and hydride phases of palladium, (ii) compare the H_2 partial pressure at which occursthe phase transition with that obtained in static conditions,[30, 31] and (iii) obtain the spectroscopic and structural fingerprints of the two pure states of the catalyst (hydride and metallic) for further usage in XANES analysis (vide infra). Then, the H_2 flow (blue) was set to 5 mL/min and C_2H_4 flow (red) was increased stepwise preserving the total flow at 50 mL/min by simultaneous tuning of He flow (red, region II in Figure 1). Finally, a similar procedure was applied but with H_2 flow of 10 mL/min (region III in Figure 1). The percentage yield of ethane, estimated based on the ratio of m/Z = 30 and 28 signals, is shown by green line in Figure 1a (see values at right ordinate axis).

Figure 1b summarizes the results of the analysis of the EXAFS and XRPD data, collected quasi-simultaneously within the same experiment. In particular, it reports the first shell Pd–Pd interatomic distances as determined from EXAFS (purple circles, left ordinate axis) and the cell parameter as obtained from XRPD (brown squares, right ordinate axis). In the region I, the catalyst was initially exposed to 50 mL/min flux of pure He. Both EXAFS and XRPD indicate that the palladium phase is in the metallic state. Then, the helium flux was decreased to 47 mL/min and 3 mL/min of H_2 was introduced. At the successive steps, the hydrogen flux was kept at 3 mL/min and the helium flux was being decreased down to 0. The XRPD was measured at every experimental point showing a gradual increase of the cell parameter with a characteristic α- to β-hydride phase transition in the region corresponding to a H_2 partial pressure of 100-150 mbar. The position of the phase transition is similar to that obtained in static conditions[30] and was independently checked in the flow conditions but keeping the constant total flux (See Figure S3 of ESI). EXAFS data were collected in the selected points and the obtained Pd-Pd interatomic distances follow a similar trend as the cell parameter determined by XRPD. However, the interatomic distances are systematically lower than those calculated based on XRPD cell

parameters. This can be explained by smaller interatomic distances in the surface regions of the NPs, compared to the bulk, which affect EXAFS data, but do not contribute to XRPD peaks.[30]

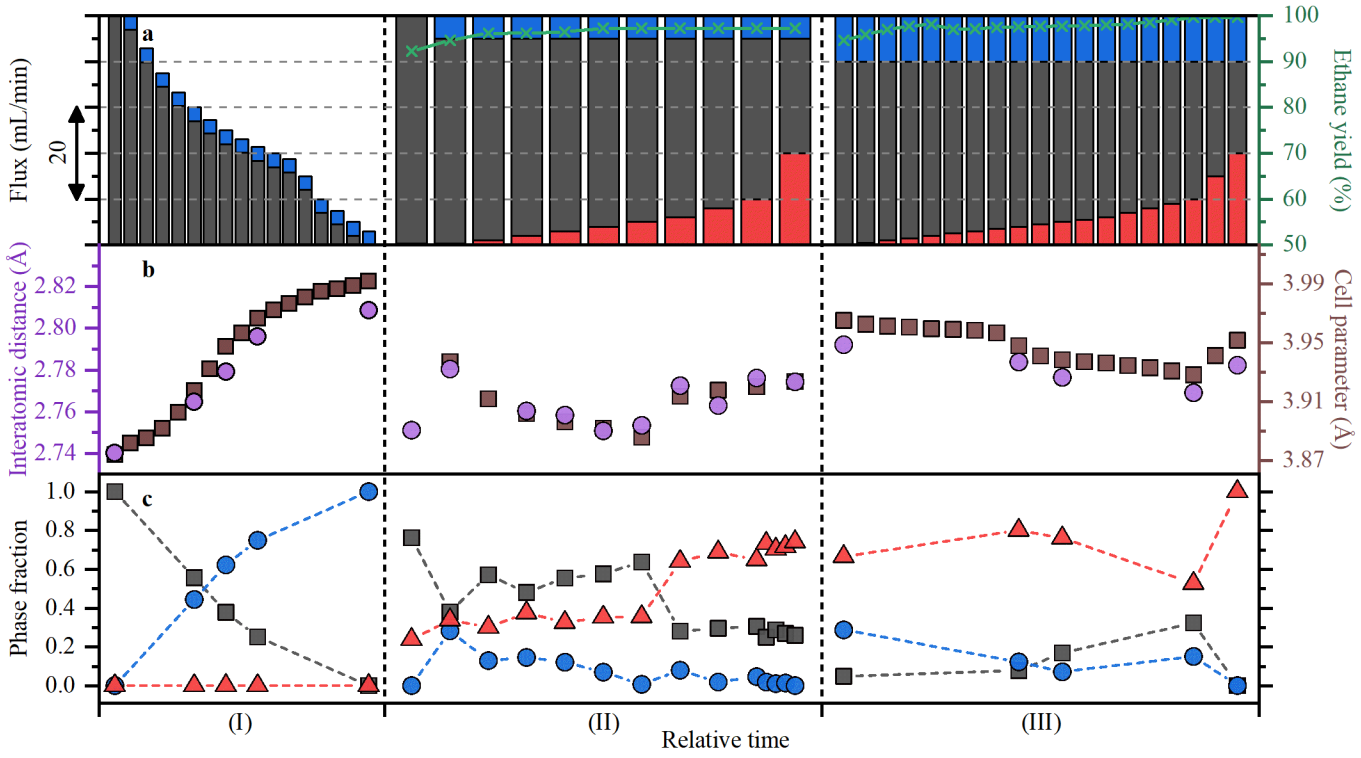

Figure 1. (a) The adjusted He, H_2, and C_2H_4 flows (black, blue, and red columns, respectively, left ordinate axis). The percentage yield of ethane is shown by green line with crosses with corresponding values in the right ordinate axis (b) Evolution of the first shell Pd–Pd interatomic distances from EXAFS (purple circles, left ordinate axis) and cell parameter from XRPD (brown squares, right ordinate axis). (c) Evolution of metallic (black squares), hydride (blue circles) and carbide (red triangles) components of palladium from XANES.

In the region II, both EXAFS and XRPD results follow a similar trend. The starting state of the catalyst in pure He is characterized by a slightly increased $R_{Pd\text{-}Pd}$ = 2.75 Å, compared to 2.74 Å in the initial state in the region I. Although the difference is within the precision of EXAFS method, its reason will be explained after the analysis of XANES data (vide infra). After addition of 5 mL/min H_2, the $R_{Pd\text{-}Pd}$ value increases to 2.78 Å, which is smaller than that for pure hydride phase (2.81 Å) and can be explained by the fact that the resulting H_2 partial pressure (100 mbar) corresponds to the phase transition region. The successive addition of C_2H_4 further decreases the $R_{Pd\text{-}Pd}$ (and cell parameter), due to conversion of C_2H_4 to C_2H_6 which decreases the partial pressure of H_2. However, even at 1:1 ethylene to hydrogen ratio with almost 100 % conversion, the $R_{Pd\text{-}Pd}$ values are bigger than 2.74 Å, indicating that the catalyst is not in the pure metallic phase. In the excess of C_2H_4 (last 4 points in the region II), the $R_{Pd\text{-}Pd}$ values increase, indicative of carbide formation. In the whole range of ethylene to hydrogen ratios, the ethane yield is close to 100%, being slightly lower in the region with big excess of H_2, which correlates with previous findings.[15, 32, 33]

When the H_2 flow is doubled to 10 mL/min (region III), both the interatomic distances and cell parameter increase to values which are only 0.6% smaller compared to pure palladium hydride. Irrespective of the ethylene to hydrogen ratios adopted in the region III, the interatomic distances

and cell parameter do not decrease below the values obtained at the end of the region II, which indirectly indicates that a stable carbide phase might have been formed.

To shed light on the phase transformations occurring during the catalytic reaction, XANES region of the absorption spectra was considered. At the first step, the whole series of XANES data (Figure S4 of ESI) was analyzed by means of PCA, which revealed the presence of three independent components (Figure S5 of ESI). The SIMPLISMA approach was then applied to extract the three components, which were interpreted as metallic, hydride and carbide species based on their spectral features (Figure S6). The linear combination fit (LCF) to the experimental data provided the relative concentration of the above phases along the experimental procedure (Figure 1c). Supporting the EXAFS and XRPD results, the region I is characterized by a phase transition from pure metallic to pure hydride phase, with the third, carbide, component being equal to zero.

In the beginning of region II, the amount of carbide is ca. 25% already in the first point. This can be explained by the presence of small traces of C_2H_4 in the gas line due to the fact that in the region I, both MFC and the valve of the C_2H_4 line were closed (See Figure S1 of ESI), while before the measurements in the region II, the valve was open and the MFC allowed passing a small amounts of ethylene, even though its setpoint was 0. According to MS reading, the absolute amount of C_2H_4 in the resulting gas flow was below 0.3 mL/min. However, even such small amount immediately reacts with the catalyst forming a carbide phase. This also explains the higher values of interatomic distances for the starting point of the region I discussed above. After addition of H_2, a concentration of hydride phase of ca. 30% was detected, with ca. 30% and 40%, of carbide and metallic phases, respectively. Upon increase of C_2H_4, the hydride component gradually decreases to zero, resulting in the mixture of carbide and metallic phases, with concentration of carbide of ca. 35% and 75% at ethylene to hydrogen ratios of 1:1 and 4:1, respectively.

The starting point of region III is characterized by a mixture of hydride and carbide components (30% and 65%, respectively), with 5% of the metallic one, which means that only a small decrease of carbide with respect to the final point of the region II occurs even in the absence of ethylene and a continuous flow of 20% H_2/He. Thus, XANES proves the formation of stable and irreversible carbide, which also explains why the biggest interatomic distances in the region III are smaller than that in pure hydride phase, and the smallest observed distances are higher than in the pure metallic phase.

3.2. Phase transition in the spent catalyst followed by XRPD

After the procedure described in Section 3.1, the spent catalyst was exposed to 10 mL/min of ethylene and the hydrogen flux was increased from 10 to 20 mL/min. The evolution of the XRPD patterns is shown in Figure 2a (from black to blue). The starting point is characterized by a single phase with the cell parameter a = 3.980 ± 0.001 Å, which can be assigned to a palladium carbide based on XANES data (Figure 1c, region III). The increase of H_2 flow leads to a gradual shift of the XRPD peaks towards higher 2θ values, indicating a lattice contraction. The Rietveld refinement (Figure 2b) revealed the coexistence of two phases. The first one (red squares) is characterized by a stable lattice parameter of ca. 3.92 Å. The second (blue squares) has a starting lattice parameter of 3.98 Å, which gradually increases to ca. 4.03 Å. Due to the decreasing fraction of the second

phase from 100 to 12%, the resulting averaged cell parameter (green circles) decreases to 3.932 ± 0.001 Å.

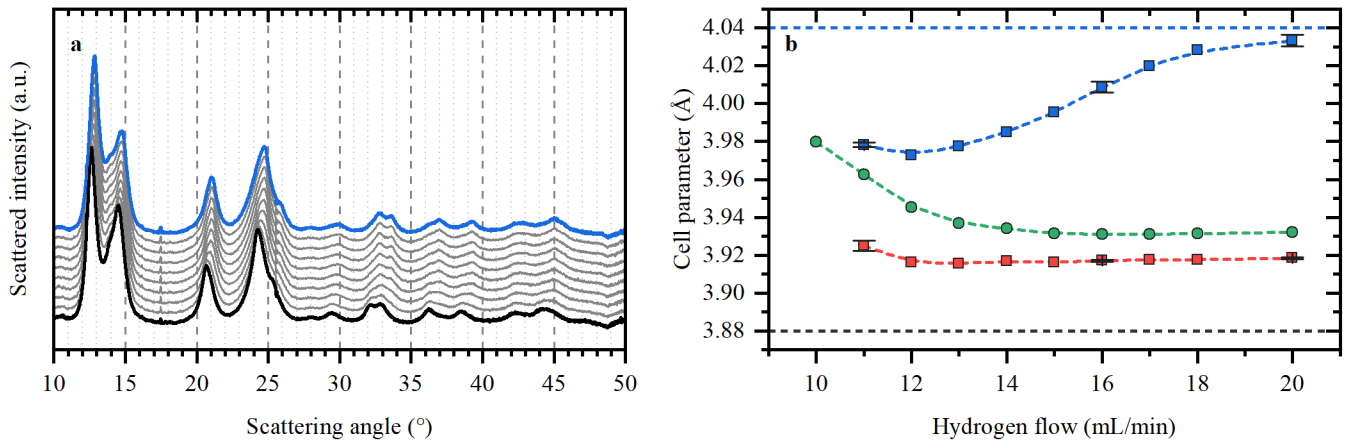

Figure 2. (a) The series of XRPD patterns collected for the used catalyst upon increasing H_2 flow from 10 (black) to 20 (blue) mL/min, at constant C_2H_4 flow of 10 mL/min. (b) Cell parameters of the two phases (red and blue squares) and they weighted average (green circles) obtained from the Rietveld refinement as a function of hydrogen H_2 flow. Error bars are shown at selected points. The horizontal black and blue lines correspond to the expected cell parameters for metallic and hydride phases, respectively.

4. Discussion

The combination of three experimental techniques, XRPD, EXAFS and XANES, applied in quasi-simultaneous conditions, allowed constructing a complete picture of the evolution of the catalyst's structure under reaction conditions. Even small concentrations of ethylene result in immediate and almost irreversible formation of palladium carbide whose concentration further increases during the reaction. The obtained results indicate that the structure of the Pd phase in a catalyst continuously exposed to hydrogen/ethylene/ethane reaction mixtures mainly corresponds to palladium carbide. In contrast to several reports,[5-8] the formation of the carbide phase does not decrease the catalyst activity in ethylene to ethane conversion, which becomes even comparing with increasing carbide concentration.

The XRPD data reported in Figure 1b indicate that in a spent catalyst, new stable palladium phases can be formed with the cell parameters different from those of α- and β-hydrides and metallic palladium. While the phase transitions with mixed-phase regions are clearly observed e.g. in the middle of region III in Figure 1b.

Exposure of the spent catalyst to an excess of hydrogen led to an unusual contraction of the cell parameter (Figure 2b). Instead of formation of palladium hydride or a mixed hydride-carbide phase with increased cell parameter, as in the beginning of region III in Figure 1b, the averaged cell parameter gradually decreases with increasing hydrogen pressure. However, with one of the phases (blue squares in Figure 2b) demonstrate an increase of the cell parameter exactly in the region which corresponds to the similar H_2 partial pressure (considering the full ethylene conversion to ethane) range as for pure metal-hydride phase transition presented in the region I of Figure 1. The possible explanation of this phenomena may by in the partial substitution of the

carbon impurities by hydrogen, which leads to a co-existence of a less concentration PdC_x phase and β-hydride. The stable width of XRPD peaks indicates that these phases are most likely formed in different participles, rather than co-exist in single ones.

5. Conclusions

In conclusion, we have performed a detailed characterization of a carbon-supportedpalladium-based catalyst during the hydrogenation of ethylene to ethane in different reaction conditions by simultaneously applying XRPD, EXAFS and XANES. The synergetic combination of the three techniques gives complementary information about atomic and electronic structure of palladium nanoparticles resulting in a comprehensive understanding, which could not be achieved by application of any of the above techniques separately. We confirmed the irreversible formation of palladium carbides under reaction conditions, but also showed that this process does not reduce the catalytic activity. Finally, we have found an abnormal increase of the cell parameter with the increasing hydrogen pressure in the spent catalyst. The analysis of the XRPD data suggested that this behaviour can be explained by a phase transition between two different carbide phases with formation of a hydride one. However, this phenomenon could be a subject of further investigation and discussion.

Conflicts of interest

Authors declare no conflicts of interest.

Acknowledgments

We are deeply indebted with Professor Carlo Lamberti, who supported us by wise advices and bright ides at all stages of this investigation. A.L.B., O.A.U., A.A.G, and A.V.S. acknowledge the Russian Ministry Science and Higher Education for the financial support (Project RFMEFI58417X0029, Agreement 14.584.21.0029). We are thankful to Vladimir Dmitriev, Herman Emerich, and Wouter van Beek for their support during the experiment performed at BM31.

Author contributions

A.L.B., J.A.B., E.G. and A.V.S. contributed to designing the experiment and gaining the beamtime at ESRF. R.P. made the chemical synthesis of the catalyst. A.L.B., A.A.G., K.L. and M.B. participated in the synchrotron experiment at ESRF. A.L.B. and O.A.U. performed the data analysis.

Notes and references

1 M. Armbrüster, M. Behrens, F. Cinquini, K. Föttinger, Y. Grin, A. Haghofer, B. Klötzer, A. Knop-Gericke, H. Lorenz, A. Ota, S. Penner, J. Prinz, C. Rameshan, Z. Révay, D. Rosenthal, G. Rupprechter, P. Sautet, R. Schlögl, L. Shao, L. Szentmiklósi, D. Teschner, D. Torres, R. Wagner, R. Widmer and G. Wowsnick, *ChemCatChem*, 2012, **4**, 1048-1063.

2 A. Borodziński and G. C. Bond, *Catalysis Reviews*, 2006, **48**, 91-144.

3 A. Borodziński and G. C. Bond, *Catalysis Reviews*, 2008, **50**, 379-469.

4 Á. Molnár, A. Sárkány and M. Varga, *Journal of Molecular Catalysis A: Chemical*, 2001, **173**, 185-221.

5 S. Shaikhutdinov, M. Heemeier, M. Bäumer, T. Lear, D. Lennon, R. J. Oldman, S. D. Jackson and H. J. Freund, *Journal of Catalysis*, 2001, **200**, 330-339.

6 D. Teschner, J. Borsodi, Z. Kis, L. Szentmiklósi, Z. Révay, A. Knop-Gericke, R. Schlögl, D. Torres and P. Sautet, *The Journal of Physical Chemistry C*, 2010, **114**, 2293-2299.
7 D. Teschner, J. Borsodi, A. Wootsch, Z. Revay, M. Havecker, A. Knop-Gericke, S. D. Jackson and R. Schlögl, *Science*, 2008, **320**, 86-89.
8 D. Teschner, Z. Revay, J. Borsodi, M. Havecker, A. Knop-Gericke, R. Schlogl, D. Milroy, S. D. Jackson, D. Torres and P. Sautet, *Angewandte Chemie*, 2008, **47**, 9274-9278.
9 M. W. Tew, M. Janousch, T. Huthwelker and J. A. van Bokhoven, *Journal of Catalysis*, 2011, **283**, 45-54.
10 M. W. Tew, M. Nachtegaal, M. Janousch, T. Huthwelker and J. A. van Bokhoven, *Physical Chemistry Chemical Physics*, 2012, **14**, 5761-5768.
11 A. Borodziński, R. Duś, R. Frąk, A. Janko, W. Palczewska, G. Bond, P. Wells and F. Tompkins, 1977.
12 F. A. Lewis, 1967.
13 A. L. Bugaev, A. A. Guda, A. Lazzarini, K. A. Lomachenko, E. Groppo, R. Pellegrini, A. Piovano, H. Emerich, A. V. Soldatov, L. A. Bugaev, V. P. Dmitriev, J. A. van Bokhoven and C. Lamberti, *Catal. Today*, 2017, **283**, 119-126.
14 A. A. Skorynina, A. A. Tereshchenko, O. A. Usoltsev, A. L. Bugaev, K. A. Lomachenko, A. A. Guda, E. Groppo, R. Pellegrini, C. Lamberti and A. Soldatov, *Radiat. Phys. Chem.*, in press, **doi: 10.1016/j.radphyschem.2018.11.033**.
15 A. L. Bugaev, A. A. Guda, I. A. Pankin, E. Groppo, R. Pellegrini, A. Longo, A. V. Soldatov and C. Lamberti, *Catal. Today*, 2019, **336**, 40-44.
16 A. L. Bugaev, A. A. Guda, I. A. Pankin, E. Groppo, R. Pellegrini, A. Longo, A. V. Soldatov and C. Lamberti, *Data Brief*, 2019, **24**, 103954.
17 R. Pellegrini, G. Leofanti, G. Agostini, E. Groppo, M. Rivallan and C. Lamberti, *Langmuir*, 2009, **25**, 6476-6485.
18 G. Agostini, E. Groppo, A. Piovano, R. Pellegrini, G. Leofanti and C. Lamberti, *Langmuir*, 2010, **26**, 11204-11211.
19 G. Agostini, C. Lamberti, R. Pellegrini, G. Leofanti, F. Giannici, A. Longo and E. Groppo, *ACS Catal.*, 2014, **4**, 187-194.
20 A. Piovano, A. Lazzarini, R. Pellegrini, G. Leofanti, G. Agostini, S. Rudić, A. L. Bugaev, C. Lamberti and E. Groppo, *Adv. Condens. Matter Phys.*, 2015, **2015**, Art. n. 803267.
21 W. van Beek, O. V. Safonova, G. Wiker and H. Emerich, *Phase Transit.*, 2011, **84**, 726-732.
22 P. M. Abdala, O. V. Safonova, G. Wiker, W. van Beek, H. Emerich, J. A. van Bokhoven, J. Sa, J. Szlachetko and M. Nachtegaal, *Chimia*, 2012, **66**, 699-705.
23 B. Ravel and M. Newville, *J. Synchrotron Radiat.*, 2005, **12**, 537-541.
24 J. J. Rehr and R. C. Albers, *Rev. Mod. Phys.*, 2000, **72**, 621-654.
25 A. Martini, S. A. Guda, A. A. Guda, G. Smolentsev, A. Algasov, O. Usoltsev, M. A. Soldatov, A. Bugaev, Y. Rusalev, C. Lamberti and A. V. Soldatov, *Computer Physics Communication*, 2019, DOI: 10.1016/j.cpc.2019.107064.
26 W. Windig and D. A. Stephenson, *Analytical Chemistry*, 2002, **64**, 2735-2742.
27 J. Kieffer and D. Karkoulis, 2013.
28 G. Ashiotis, A. Deschildre, Z. Nawaz, J. P. Wright, D. Karkoulis, F. E. Picca and J. Kieffer, *Journal of Applied Crystallography*, 2015, **48**, 510-519.
29 V. Petříček, M. Dušek and L. Palatinus, *Z. Kristallogr. Cryst. Mater.*, 2014, **229**, 345–352.
30 A. L. Bugaev, A. A. Guda, K. A. Lomachenko, V. V. Shapovalov, A. Lazzarini, J. G. Vitillo, L. A. Bugaev, E. Groppo, R. Pellegrini, A. V. Soldatov, J. A. van Bokhoven and C. Lamberti, *J. Phys. Chem. C*, 2017, **121**, 18202-18213.
31 A. L. Bugaev, A. A. Guda, K. A. Lomachenko, V. V. Srabionyan, L. A. Bugaev, A. V. Soldatov, C. Lamberti, V. P. Dmitriev and J. A. van Bokhoven, *J. Phys. Chem. C*, 2014, **118**, 10416-10423.
32 U. Jung, A. Elsen, Y. Li, J. G. Smith, M. W. Small, E. A. Stach, A. I. Frenkel and R. G. Nuzzo, *ACS Catal.*, 2015, **5**, 1539-1551.
33 S. Zhao, Y. Li, D. Liu, J. Liu, Y.-M. Liu, D. N. Zakharov, Q. Wu, A. Orlov, A. A. Gewirth, E. A. Stach, R. G. Nuzzo and A. I. Frenkel, *The Journal of Physical Chemistry C*, 2017, **121**, 18962-18972.